A SPARSE ESTIMATION TECHNIQUE FOR NEAR FIELD UWB TARGET DETECTION IN MEDICAL IMAGING

N. Murtaza and J. W. Wallace

Department of Electrical Engineering, Jacobs University, Bremen,
Campus Ring 1, 28759, Bremen, Germany, Email: n.murtaza@jacobs-university.de, wall@ieee.org

I. INTRODUCTION

Ultra-wideband (UWB) sensing has been proposed as a method for performing medical monitoring and imaging tasks safely and unobtrusively, since signals are non-ionizing and very low power, and no physical contact with the subject is required [1, 2]. For optimal power collection and resolution considerations, it is advantageous for the subject to be in the near field of the UWB elements. In this work, the performance of a number of existing imaging methods is studied and it is found that the resolution is relatively poor for realistic array sizes (10 elements) and excitation bandwidths (3 GHz). Also, the existing methods have difficulty identifying targets when the imaging pixel size is too large and there are too many (5-10) targets. A sparse detection method based on linear programming is proposed that fits the response to a parametric model in an l_1-norm sense. The method accurately identifies up to 10 targets with good resolution, suggesting that this robust technique is suitable for such applications.

II. BACKGROUND

This section describes the model and tested imaging methods. In this work, boldface lowercase and capital letters are vectors and matrices, respectively, and spatial cartesian coordinates are represented by vectors.

A. Model

Figure 1 depicts the basic model assumed, where the ith antenna element is located at $\mathbf{q}_i$, the mth target (representing a feature of interest or foreign body) is at $\mathbf{r}_m$, and the imaging region is divided into $L = L_x \times L_y$ pixels with pixel centers at $\mathbf{p}_\ell$. Each antenna successively transmits a UWB signal and then receives the return waveform.

In the frequency domain, the response at the ith element is

$$y_i(\omega) = \sum_{m=1}^{M} \underbrace{h_m(\omega)s(\omega)}_{x_m(\omega)} \underbrace{\frac{\exp\left(-\frac{2j\omega}{c}\|\mathbf{q}_i - \mathbf{r}_m\|\right)}{\|\mathbf{q}_i - \mathbf{r}_m\|^2}}_{a_i(\mathbf{r}_m,\omega)} + n_i(\omega), \tag{1}$$

where ω is frequency, c is the wavespeed, $h_m(\omega)$ is the frequency response of the mth target, $s(\omega)$ is the UWB transmit signal (identical for all antennas), $\mathbf{a}(\mathbf{r}_m, \omega)$ is the near field steering vector (assuming free-space-like propagation from the antenna to the target and back), and $n_i(\omega)$ is thermal amplifier noise. Although we neglect the strong surface reflection in the present analysis, this will be the subject of later investigations.

For a single frequency ω, the relationship in vector form is $\mathbf{y} = \mathbf{A}\mathbf{x} + \mathbf{n}$. Sampling at K discrete frequencies ω_k,

$$y_{ik} = \sum_{m=1}^{M} x_{km} a_{ik,m} + n_{ik}, \tag{2}$$

where $a_{ik,m} = a_i(\mathbf{r}_m, \omega_k)$. For simplicity, we assume ideal point targets whose impulse response is just a Dirac delta in the time domain (frequency flat), so that $x_{km} = x_m$. Stacking i and k, we again have $\mathbf{y} = \mathbf{A}\mathbf{x} + \mathbf{n}$, and this is referred to as the joint space/frequency case.

The modeled covariance (either for a single frequency or the joint case) is given as

$$\mathbf{R}_y = \mathbf{A}\mathbf{R}_x\mathbf{A}^H + \sigma^2\mathbf{I}, \tag{3}$$

where $\mathbf{R}_x = \mathrm{diag}(\boldsymbol{\beta})$, $\beta_m = \mathrm{E}|x_m|^2$, it is assumed that the targets are fading and independent, and the noise is i.i.d. The assumption that the targets are fading is not very realistic, since everything in the scenario is fixed and deterministic. However, we will consider the performance of the methods for only a single realization as well, which models the deterministic case.

B. Beamforming Methods

To perform beamforming, $\mathbf{A}$ is interpreted as a near field steering vector. The steering vector for the center of the ℓth pixel is $\mathbf{a}(\mathbf{p}_\ell, \omega)$. Stacking the steering vectors for the K frequencies, we obtain a single vector $\mathbf{a}(\mathbf{p}_\ell)$. The two beamformers that are considered in this work are the Bartlett and Capon beamformers [3], given by

$$b_\ell^{\text{bart}} = \frac{\mathbf{a}^H(\mathbf{p}_\ell)\mathbf{R}_y\mathbf{a}(\mathbf{p}_\ell)}{\mathbf{a}^H(\mathbf{p}_\ell)\mathbf{a}(\mathbf{p}_\ell)} \quad \text{and} \quad b_\ell^{\text{cap}} = \frac{1}{\mathbf{a}^H(\mathbf{p}_\ell)\mathbf{R}_y^{-1}\mathbf{a}(\mathbf{p}_\ell)}. \tag{4}$$

C. Imaging Techniques

This work considers the following existing imaging techniques:

1) *Incoherent Beamforming* – In this case, relations (4) are used on each frequency separately, and the total power in each pixel is found by summing the power from all frequencies.
2) *Coherent Refocusing* – Here, the method described in [4] is used, where the response $\mathbf{y}$ at each frequency is transformed by a refocusing matrix $\mathbf{T}(\omega_0, \omega_k)$ that attempts to transform the response at frequency ω_k to the expected response at ω_0. The purpose of this transformation is to convert the wideband problem into a narrowband one.
3) *Joint Space/Frequency Beamforming* – The joint space/frequency beamformer uses the stacked steering vector for all frequency samples, generating a single pixel power using all frequencies simultaneously.

In addition, we propose a new linear programming (LP) technique that assumes that the covariance can be written as

$$\mathbf{R}_y = \sum_{\ell'=1}^{L} \mathbf{a}(\mathbf{p}_{\ell'}) g_{\ell'} \mathbf{a}^H(\mathbf{p}_{\ell'}), \tag{5}$$

where g_ℓ is the power of a potential target at the ℓth pixel. Substituting this parametric form of the covariance into the Bartlett beamformer and neglecting noise gives

$$b_\ell = \sum_{\ell'=1}^{L} \underbrace{\frac{\mathbf{a}^H(\mathbf{p}_\ell)\mathbf{a}(\mathbf{p}_{\ell'})\mathbf{a}^H(\mathbf{p}_{\ell'})\mathbf{a}(\mathbf{p}_\ell)}{\mathbf{a}^H(\mathbf{p}_\ell)\mathbf{a}(\mathbf{p}_\ell)}}_{d_{\ell\ell'}} g_{\ell'}. \tag{6}$$

Note that this last equation is in the form of a standard linear programming (LP) problem, or

$$\hat{\mathbf{g}} = \arg\min \mathbf{c}^T\mathbf{x} \quad \text{subject to} \quad \mathbf{b} = \mathbf{D}\mathbf{g}, \quad g_i \geq 0 \quad \forall i, \tag{7}$$

where $\mathbf{c}$ is the cost vector. Since an exact fit between the modeled and measured Bartlett beamformer outputs may not be possible due to deviations from the model, noise, or other system issues, small error is allowed into the fit by letting $\mathbf{b} = \mathbf{D}\mathbf{g} + \boldsymbol{\epsilon}_P - \boldsymbol{\epsilon}_M$, where $\boldsymbol{\epsilon} = \boldsymbol{\epsilon}_P - \boldsymbol{\epsilon}_M$ is the error vector. The expanded LP problem becomes

$$\mathbf{b}' = \mathbf{b} \quad \mathbf{g}' = \begin{bmatrix} \mathbf{g} \\ \boldsymbol{\epsilon}_P \\ \boldsymbol{\epsilon}_M \end{bmatrix} \quad \mathbf{D}' = [\ \mathbf{D} \quad \mathbf{I} \quad -\mathbf{I}\ ], \tag{8}$$

where $\mathbf{I}$ is an identity matrix. It has been found that minimum l_1-norm solutions, like those found with linear programming, tend to give sparse solutions, which is advantageous for this problem [5, 6]. Note that we have also tried an LP solution that fits the relation (2) directly, but this does not appear to be as stable as this beamspace form.

III. Simulations

Due to space limitations, only a small subset of the simulations can be presented. In what follows, the UWB transmit signal is assumed to be frequency flat from 3 to 6 GHz, and this band is sampled at $K = 12$ equi-distant points. The array is a uniform linear array centered at $(0, 0)$ with $N = 10$ elements and $\lambda/2$-element spacing at the center frequency of 4.5 GHz. SNR is set at 20 dB for all cases. A square imaging area is assumed to be 0.5 m from the array, having dimensions $0.5{\times}0.5$ m^2.

IV. Fluctuating Targets

First we consider the fortuitous case where targets fade (x_m are distributed as i.i.d. complex normal random variables), 100 random realizations are available to compute the covariance, and a single target occurs at exactly one of the pixel centers. Figure 2 depicts the performance of the methods for a typical realization. The incoherent Bartlett beamformer

(IB) finds the target in cross-range (angle), but not in range, since the power is added incoherently. The incoherent Capon beamformer (IC) mostly localizes the target, which is made possible by different wavefront curvatures for far and near targets. Refocusing (REF) does not seem to provide useful results, perhaps because we use a simple form of the refocusing matrix that refocuses for the "look" pixel only. The joint beamformers perform better than their incoherent counterparts, since the frequency (and therefore range) information is used coherently. Both joint Bartlett (JB) and joint Capon (JC) localize the target, with JC providing better cross-range resolution. Finally linear programming (LP) perfectly localizes the target. Due to their better performance, we will concentrate on the IC, JB, JC, and LP cases.

A more realistic case is depicted in Figure 3 where the target is no longer at a pixel center. It can be seen that JB has the same performance as before, but the IC and JC cases begin to show artifacts due to sensitivity created by the inverse of the covariance. Note that LP still adequately localizes the target.

Figure 4 depicts the results for the beamforming techniques for more targets for the JB and LP cases. Both cases provide good performance for up to 10 targets, with LP having superior resolution.

As we indicated earlier, having fluctuating targets in a medical imaging application is not very realistic, since in practice only a single realization can be observed. Figure 5 shows the results for the JB, JC, and LP cases for a single realization of the targets, where $|x_m| = 1$ and $\angle x_m$ is uniform on $(0, 2\pi)$. As this typical result indicates, both of these methods provide adequate performance for only a single realization with multiple targets. The Capon beamformer fails to work, because the covariance is rank deficient for only a single realization.

V. Conclusion

This paper studied a number of near field UWB imaging methods based on conventional beamforming techniques, where the wideband frequency information is used incoherently or coherently. Application of the methods to a scene with a small number of targets indicated that none of the existing methods exhibited both robustness and high resolution. A new linear-programming based method was developed, exhibiting robustness and high-resolution localization of the targets, indicating that the technique holds promise for UWB medical imaging and sensing applications.

References

[1] E. M. Staderini, "UWB radars in medicine," *IEEE Aerospace and Electronic Systems Magazine*, vol. 17, pp. 13–18, Jan. 2002.
[2] I. Y. Immoreev, S. Samkov, and T.-H. Tao, "Short-distance ultra wideband radars," *IEEE Aerospace and Electronic Systems Magazine*, vol. 20, pp. 9–14, June 2005.
[3] H. Krim and M. Viberg, "Two decades of array signal processing research: The parametric approach," *IEEE Signal Processing Magazine*, vol. 13, pp. 67–94, Jul. 1996.
[4] W. Zhi, F. Chin, and M.-W. Chia, "Near field imaging for breast cancer detection by UWB minimum variance beamforming," in *Proc. 2006 IEEE Intl. Conf. Ultra-Wideband*, Waltham, MA, Sept. 2006, pp. 593–597.
[5] S. S. Chen, D. L. Donoho, and M. A. Saunders, "Atomic decomposition by basis pursuit," *SIAM Review*, vol. 43, pp. 129–159, Mar. 2001.
[6] J. Wallace, H. Özcelik, M. Herdin, E. Bonek, and M. Jensen, "A diffuse multipath spectrum estimation technique for directional channel modeling," in *Proc. 2004 IEEE Intl. Conf. Commun.*, vol. 6, Paris, France, Jun. 20-24 2004, pp. 3183–3187.

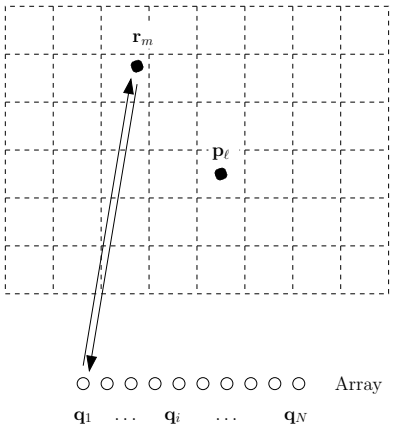

Fig. 1. Model scenario for wideband near field imaging

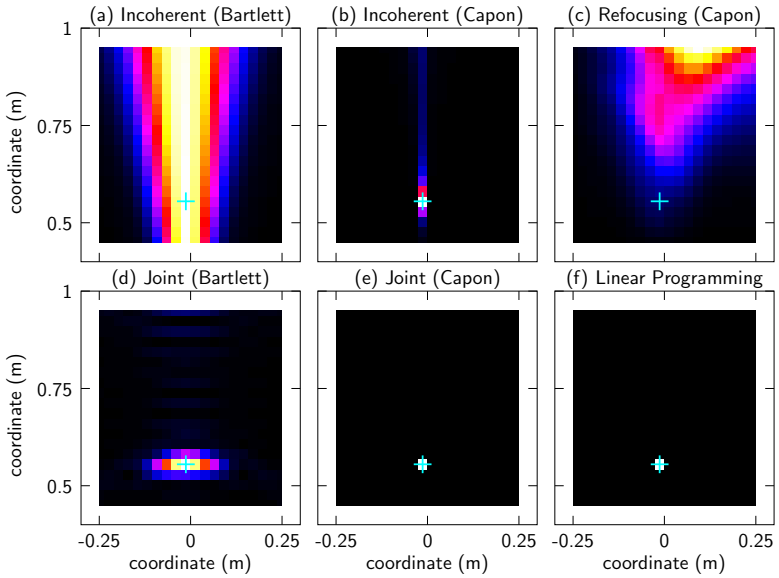

Fig. 2. Simulation of the various methods for the ideal case of a single target whose position coincides with a pixel center

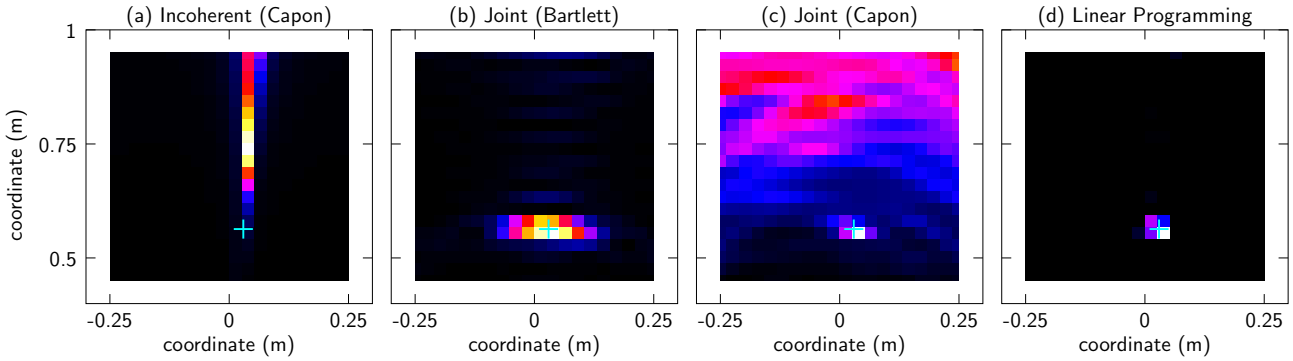

Fig. 3. Simulation of the various methods for a single target at a random position

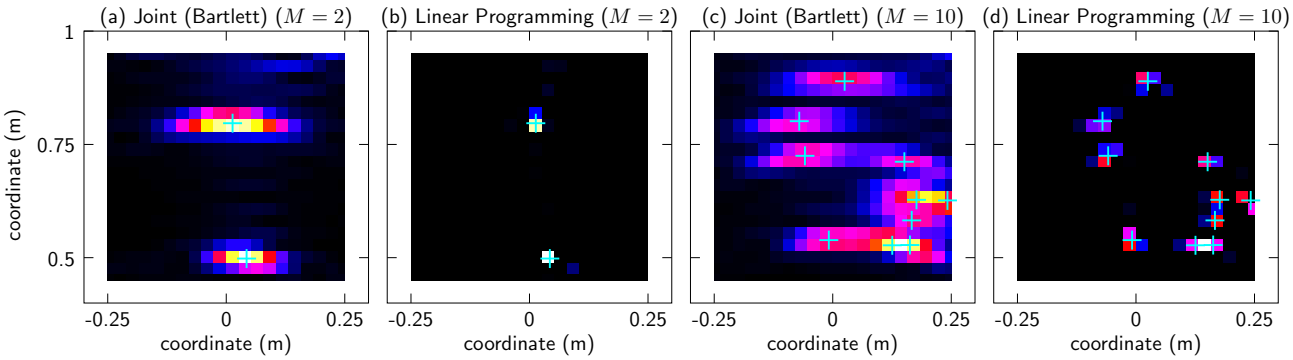

Fig. 4. Simulation of joint Bartlett and linear programming for 2 and 10 targets

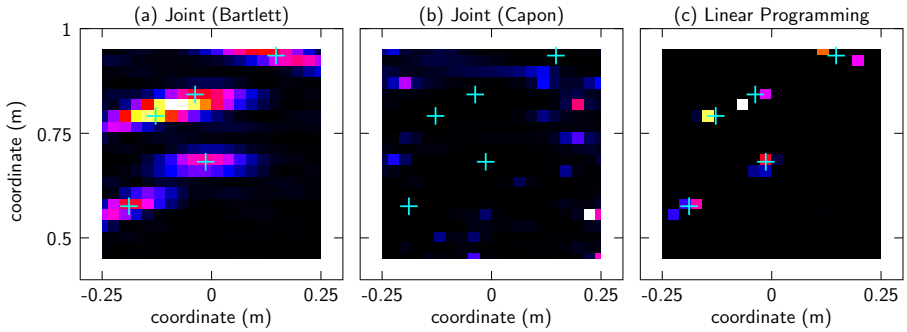

Fig. 5. Simulation of joint Barlett, joint Capon, and linear programming methods for 5 targets and only a single realization (observation)